Title

Changes in profile distribution and chemical properties of natural nanoparticles in paddy soils as affected by long-term rice cultivation

Journal

Pedosphere, 31(5)

ISSN

1002-0160

Authors

HUANG, Dan
Xinyu, ZHU
Baile, XU
et al.

Publication Date

2021-10-01

DOI

10.1016/s1002-0160(21)60015-2

Peer reviewed

Pedosphere **31**(5): 659–669, 2021
doi:10.1016/S1002-0160(21)60015-2
ISSN 1002-0160/CN 32-1315/P

Published by Elsevier B.V. and Science Press

PEDOSPHERE

www.elsevier.com/locate/pedosphere

Changes in profile distribution and chemical properties of natural nanoparticles in paddy soils as affected by long-term rice cultivation

Dan HUANG[1,2], Xinyu ZHU[1,2], Baile XU[1,2], Yan HE[1,2], Mingkui ZHANG[1,2], Fei LIU[1,2], Zhenghua LIAN[1,2], Randy A. DAHLGREN[3], Philip C. BROOKES[1,2] and Jianming XU[1,2,*]

[1]*Institute of Soil and Water Resources and Environmental Science, College of Environmental and Resource Sciences, Zhejiang University, Hangzhou 310058 (China)*
[2]*Zhejiang Provincial Key Laboratory of Agricultural Resources and Environment, Hangzhou 310058 (China)*
[3]*Department of Land, Air and Water Resources, University of California – Davis, Davis CA 95616 (USA)*

(Received April 28, 2020; revised June 5, 2020)

ABSTRACT

Systematic studies on the genesis, properties, and distribution of natural nanoparticles (NNPs) in soil remain scarce. This study examined a soil chronosequence of continuous paddy field land use for periods ranging from 0 to 1 000 years to determine how NNPs in soil changed at the early stages of soil genesis in eastern China. Soil samples were collected from coastal reclaimed paddy fields that were cultivated for 0, 50, 100, 300, 700, and 1 000 years. Natural nanoparticles were isolated and characterized along with bulk soil samples (< 2-mm fraction) for selected physical and chemical properties. The NNP content increased with increasing soil cultivation age at 60 g m^{-2} $year^{-1}$, which was related to decreasing soil electrical conductivity (172–1 297 μS cm^{-1}) and NNP zeta potentials (from −22 to −36 mV) with increasing soil cultivation age. Changes in several NNP properties, such as pedogenic iron oxide and total organic carbon contents, were consistent with those of the bulk soils across the soil chronosequence. Notably, changes in NNP iron oxide content were obvious and illustrated active chemical weathering, pedogenesis, and potential impacts on the microbial community. Redundancy analysis demonstrated that the soil cultivation age was the most important factor affecting NNP properties, contributing 60.7% of the total variation. Cluster and principal component analysis (PCA) revealed splitting of NNP samples into age groups of 50–300 and 700–1 000 years, indicating rapid evolution of NNP properties, after an initial period of desalinization (approximately 50 years). Overall, this study provides new insights into NNP evolution in soil during pedogenesis and predicting their influences on agriculture and ecological risks over millennial-scale rice cultivation.

Key Words: natural nanoparticle evolution, soil chronosequence, soil cultivation age, soil genesis, soil nanoparticles

Citation: Huang D, Zhu X Y, Xu B L, He Y, Zhang M K, Liu F, Lian Z H, Dahlgren R A, Brookes P C, Xu J M. 2021. Changes in profile distribution and chemical properties of natural nanoparticles in paddy soils as affected by long-term rice cultivation. *Pedosphere*. **31**(5): 659–669.

INTRODUCTION

Natural nanoparticles (NNPs), defined as naturally produced particles < 100 nm, are ubiquitous and display a variety of chemical and mineralogical compositions (Hochella *et al*., 2008; Li *et al*., 2012; Zhu *et al*., 2017). The annual production of NNPs through biogeochemical processes is estimated to be several thousands of teragrams (1 Tg = 1 million metric tons) (Hochella *et al*., 2015). Soil NNPs have a disproportionate importance relative to their abundance with respect to several crucial ecological services (Theng and Yuan, 2008; Hochella *et al*., 2019), including influencing soil hydrological properties (Zhang *et al*., 2016), long-distance translocation of soil particles (Rod *et al*., 2018), and sorption and transport of contaminants and nutrients in the subsurface environment (Bakshi *et al*., 2015; Taghipour and Jalali, 2018; Liu F *et al*., 2019). These widely distributed soil particles, including mineral weathering products and organic particles derived from the decay of plant and microbial debris, have a complex composition that is affected by soil formation pathways (Li *et al*., 2012; Van Den Bogaert *et al*., 2015). The recent development of enhanced NNP extraction and characterization methods provides a strong foundation for further studies on NNPs (Bakshi *et al*., 2014; Liu F *et al*., 2019).

Properties of NNPs, at the nano-scale of 1–100 nm, may be very different from those of soil colloids (Taghipour and Jalali, 2018). Our previous study has demonstrated that soil NNPs have a higher mobility than the clay fraction (Liu *et al*., 2018). Moreover, NNPs act as carriers for contaminants and thus likely facilitate the spread of contaminants, posing a potential risk to groundwater (Liu F *et al*., 2019; Wang *et al*., 2019; Xu *et al*., 2019). Thus, it is important to study the soil physical and chemical properties across a wide range of spatial and temporal scales to better understand soil physicochemical processes resulting in NNP formation (Hochella *et al*., 2019). Given the high reactivity of NNPs,

*Corresponding author. E-mail: jmxu@zju.edu.cn.

they play a disproportionate role and therefore require special attention, especially regarding their fate and transport over pedogenic time scales.

As the dominant agricultural soils worldwide, paddy soils occupy 11% (1 956 000 km^2) of cultivated land area and provide a fundamental food source (Leff *et al.*, 2004; Song *et al.*, 2017). Paddy soils undergo complex redox conditions and variations in organic matter during the rice cultivation processes (Jiang J *et al.*, 2017), which likely makes the distribution and properties of NNPs different from those of their bulk soils. However, the properties, fate, and environmental influence of NNPs in paddy soils have been the subject of few studies, thereby warranting further investigation.

The soil physical and biogeochemical properties are particularly dynamic in paddy soils due to long-term, managed oxidation and reduction cycles. Previous studies have mainly focused on organic carbon (C) dynamics (Wei *et al.*, 2018), greenhouse gas emissions (Zhu *et al.*, 2018; Liu G *et al.*, 2019; Qian *et al.*, 2020), and soil microbial properties (Watanabe *et al.*, 2020). In addition, puddling of paddy soils strongly influences soil structure characteristics (Zhou *et al.*, 2016) with structure destruction reducing infiltration, which can increase surface runoff and loss of NNPs with associated contaminants (Zhang and Gong, 2003). While some studies have examined soil clay mineralogy in response to paddy management (Wissing *et al.*, 2014; Han *et al.*, 2015), few previous studies have investigated soil NNP dynamics over long time periods (up to 1 000 years) using a well-constrained soil chronosequence approach (Huang *et al.*, 2015). Long-term studies on soil NNPs provide novel insights into understanding NNP genesis, transformations, and property changes in response to long-term paddy management.

Therefore, a paddy soil chronosequence of a coastal area in eastern China, where soils were created from the reclamation of alluvial-marine sediments over the millennial time scale (0 to 1 000 years), was established for investigation. Based on characteristics of bulk soil and NNPs in soil over the 1 000-year-long period, we sought to address the following three hypotheses: i) the distribution and properties of soil NNPs vary under long-term paddy management; ii) soil NNP properties are related to changes in bulk soil properties over time; and iii) soil cultivation age and depth are the dominant factors controlling variations in NNP properties. Our main objective was to identify how the abundance and characteristics of paddy soil NNPs changed during long-term (1 000 years) rice cultivation.

MATERIALS AND METHODS

Study sites and sample collection

The study was conducted in the coastal area of Cixi on the southern bank of Hangzhou Bay, Zhejiang Province, eastern China (Fig. S1, see Supplementary Material for Fig. S1). The area has a typical subtropical monsoon climate with a mean annual precipitation of 1 325 mm and a mean annual temperature of 16.3 °C (Liu Y *et al.*, 2019). The Qiantang River flows downstream to Hangzhou Bay and the East China Sea at an average flow of approximately 1 050 $m^3\ s^{-1}$ and with a mean sediment transport of 212 kg s^{-1} (Guo *et al.*, 2012). Sediment input from the Yangtze River to the north also affects the sedimentation of Hangzhou Bay (Xie *et al.*, 2009, 2017); the dominant clay mineral of the sediment/soil is illite (Wissing *et al.*, 2014). Over the last thousand years, land reclamation has contributed to growth of tidal flats at an average rate of 20 m $year^{-1}$ (Xie *et al.*, 2009). Dikes were built in different periods to protect the newly developed lands from the tide. Local records accurately document the building of individual dikes, allowing us to select sites representing a specific soil chronosequence (Chen *et al.*, 2011). We selected sites that were cultivated for 0, 50, 100, 300, 700, and 1 000 years (Table SI, see Supplementary Material for Table SI). The 0-year site was a newly developed wetland covered with weeds and reeds, while all other sites were paddy fields used for long-term rice cultivation.

For each cultivation age (time since start of paddy management), triplicate soil profiles from various depths were collected within a plot of 100–200 m^2. Each profile was divided into five depth increments: 0–20, 20–40, 40–60, 60–80, and 80–100 cm, except for the wetland (0-year cultivation), where the profile was shallow and only the 0–20 cm depth was sampled. All soil samples were air dried, gently crushed, sieved to < 2 mm, and stored for subsequent analyses.

Characterization of soils

Selected soil properties were analyzed following protocols from the National Standards of China (Li *et al.*, 2012); specific methods are provided in SI (see Supplementary Material for SI). After removal of organic matter and total free iron oxides (Fe_d), the mineral composition of the clay fraction (< 2 μm) was determined using XRD analysis (detailed procedures are presented in SI). Based on the identified soil properties, the soils were classified as Fluvaquentic Endoaquolls (Soil Survey Staff, 2014).

Extraction and characterization of NNPs

We used ultrasonic dispersion and centrifugation to isolate NNPs from the soil samples following previously established methods (Li *et al.*, 2012; Bakshi *et al.*, 2014). An ultrasonic processor VCX750 (Sonics, Newtown, USA) was used to disperse NNP samples at an energy level of 60 000 J. A 3-g soil sample was added to 80 mL deionized water and sonicated for 30 min at a temperature less than 25 °C. To reflect the potential for natural mobilization of NNPs, no

chemicals were added to assist dispersion. After ultrasonic dispersion, the suspension was passed through a 50-μm sieve and centrifuged (Sorvall ST16R, Thermo, Osterode, Germany) three times at 3 500 g for 24 min to collect NNPs (Li *et al*., 2012). The entire extraction process (ultrasonic dispersion and centrifugation) was repeated 10 times to collect sufficient NNP mass for subsequent analyses. After centrifugation, we collected supernatants in 100-mL glass bottles for particle size and zeta potential analyses. The NNP extraction was achieved in all soils, except for the wetland soil that yielded virtually no NNP particles. Dynamic light scattering (ZetaSizer Nano ZS90, Malvern, Worcestershire, UK) revealed no aggregation of the extracted NNPs.

After collection of NNPs, we immediately measured their hydrodynamic size in triplicate using dynamic light scattering in disposable sizing cuvettes (DTS0012, Sarstedt, Nümbrecht, Germany). Zeta potential was measured at 25 °C with a ZetaSizer Nano ZS90 equipped with DTS1060c zeta cells (Malvern Panalytical, Malvern, UK). Samples were equilibrated for 120 s, and zeta potential measurements were repeated in triplicate.

We used transmission electron microscopy (TEM) to examine the size and morphology of the NNPs. An aliquot of NNP suspension was placed on a 230-mesh copper film (ZJKY Technology, Beijing, China) and air dried prior to imaging with a JEOL-JEM-1230 TEM (JEOL, Tokyo, Japan) at 100 kV. We characterized the mineralogical composition of the NNP fraction with a Bruker D8 Advance XRD (Bruker AXS, Madison, USA).

The NNP samples were weighed after drying at 40 °C for 24 h. The elemental composition of the NNPs, including total iron (Fe_t), total manganese (Mn_t), total aluminum (Al_t), total silicon (Si_t), Fe_d, poorly crystalline iron oxides (Fe_o), and crystalline iron oxides (Fe_{do}), was determined as described in SI for the bulk soil fraction (< 2 mm). Total organic C (TOC) was determined with a Multi N/C 3100 TOC analyzer (Analytik Jena, Jena, Germany). All measurements were performed in triplicate.

Statistical analyses

Linear regressions between the NNP stocks of the entire 1-m soil profile and the soil cultivation age were obtained using OriginPro 2016 software (OriginLab Corp., Northampton, USA). Linear correlations between the bulk soil (< 2 mm) and NNP properties were determined using Pearson correlation coefficients (r) for the complete dataset ($n = 25$) with SPSS 16.0 (IBM Corp., Armonk, USA). We performed a network analysis based on the Pearson correlation analysis between the bulk soil and NNP properties along with the Bonferroni correction using Gephi 0.9.2 (Bastian *et al*., 2009).

We investigated relationships between the bulk soil and NNP properties using multivariate analyses with CANOCO 5.0 and R-base packages. Canonical redundancy analysis (RDA) was used to test which bulk soil properties significantly explained the variation in NNP properties. All measured soil properties were $\log_{10}$-transformed (except pH) to improve normality and homoscedasticity for multivariate statistical analysis. Collinearity of bulk soil properties was investigated using variance inflation factor (VIF), and collinear variables with VIF > 20 were excluded. Significant variables for analysis were pre-selected from groups of variables (*i.e*., soil cultivation age, sand, silt, bulk density, pH, electrical conductivity (EC), cation exchange capacity (CEC), the cations potassium (K^+), sodium (Na^+), magnesium (Mg^{2+}), and calcium (Ca^{2+}) extracted with ammonium acetate, contents of Fe_t, Mn_t, Al_t, Si_t, Fe_d, and Fe_o, total titanium (Ti_t) and zirconium (Zr_t) contents, and Ti/Zr mass ratio in the silt fraction) using forward model selection. The significance levels of the RDA models and selected variables were determined from the Monte Carlo test (999 permutations) at $P < 0.05$ for each group. The respective effects of variables or groups of variables on the variation in NNP properties were further investigated using canonical variation partitioning.

We assessed changes in the bulk soil and NNP properties of different soil cultivation age groups using hierarchical cluster analysis of standardized values for each soil depth. Principal component analysis (PCA) was applied to further explore similarities among age/depth groups based on NNP properties.

RESULTS

Characterization of natural nanoparticles

Soil NNP content ranged from 2 to 6.2 g kg^{-1} after 50–1 000 years of rice cultivation (Table I). No NNPs were attained in the wetland soil, which showed no evidence of soil horizon development based on field morphological investigations. The NNP content was distinctly enhanced in subsoil (40–100 cm) horizons of the older soils (700–1 000 years), but was more uniformly distributed within the 1-m profiles in the younger soils (50–300 years) (Fig. 1a). Bulk soil properties from the 1 000-year soil chronosequence are listed in Table SII (see Supplementary Material for Table SII) and a detailed description of their variations across the chronosequence is presented in SI. Compared to the younger soils, the older soils had generally higher clay contents (Table SII). All NNPs were negatively charged based on zeta potential measurements, and zeta potential significantly decreased with increasing cultivation age ($r = -0.75$, $P < 0.01$). The mineralogical composition of all NNPs was constant, with illite and montmorillonite being dominant, which was consistent with the soil clay fraction (Fig. S2, see Supplementary Material for Fig. S2). A significant increase,

TABLE I

Properties of natural nanoparticles (NNPs) extracted from soil samples in the 1-m profiles under rice cultivation across a 1 000-year chronosequence in the coastal area of Cixi on the southern bank of Hangzhou Bay, Zhejiang Province, eastern China

Soil cultivation age	Soil depth	NNP mean size	NNP content	NNP property[a)]							
				Zeta potential	TOC	Fe_t	Fe_d	Fe_o	Mn_t	Al_t	Si_t
years	cm	nm	g kg^{-1}	mV	g kg^{-1}						
50	0–20	84 ± 10[b)]	3 ± 1	−23 ± 1	35 ± 6	74 ± 3	22 ± 4	18 ± 5	1.14 ± 0.09	105 ± 3	194 ± 7
	20–40	87 ± 2	2 ± 1	−23 ± 1	31 ± 5	65 ± 3	13 ± 2	8 ± 2	1.43 ± 0.16	105 ± 4	208 ± 8
	40–60	97 ± 13	5 ± 2	−25 ± 1	21 ± 4	87 ± 4	24 ± 3	13 ± 2	1.41 ± 0.12	111 ± 4	201 ± 8
	60–80	97 ± 14	3 ± 1	−24 ± 1	13 ± 3	74 ± 1	21 ± 5	9 ± 3	0.90 ± 0.13	109 ± 4	211 ± 10
	80–100	91 ± 25	9 ± 3	−25 ± 1	17 ± 4	71 ± 7	36 ± 6	13 ± 3	0.71 ± 0.12	104 ± 6	218 ± 5
100	0–20	89 ± 12	19 ± 6	−22 ± 0	32 ± 5	72 ± 3	18 ± 3	15 ± 3	1.20 ± 0.05	110 ± 2	205 ± 15
	20–40	91 ± 20	3 ± 1	−25 ± 3	25 ± 5	56 ± 4	15 ± 4	7 ± 1	1.00 ± 0.13	107 ± 3	228 ± 8
	40–60	95 ± 14	8 ± 2	−23 ± 3	22 ± 2	60 ± 5	22 ± 2	13 ± 3	0.77 ± 0.06	106 ± 3	207 ± 8
	60–80	97 ± 8	6 ± 2	−22 ± 0	15 ± 3	87 ± 3	24 ± 3	16 ± 4	1.24 ± 0.10	103 ± 4	182 ± 9
	80–100	82 ±10	11 ± 3	−23 ± 1	18 ± 2	69 ± 4	31 ± 3	18 ± 5	1.05 ± 0.08	104 ± 3	204 ± 10
300	0–20	82 ± 8	16 ± 4	−29 ± 4	38 ± 2	91 ± 4	28 ± 3	15 ± 4	0.77 ± 0.15	107 ± 5	218 ± 10
	20–40	81 ± 10	5 ± 1	−29 ± 3	25 ± 5	70 ± 6	21 ± 5	15 ± 5	0.65 ± 0.07	105 ± 3	199 ± 12
	40–60	89 ± 3	15 ± 0	−28 ± 4	14 ± 4	67 ± 5	31 ± 2	12 ± 1	0.48 ± 0.07	99 ± 4	222 ± 8
	60–80	88 ± 7	11 ± 2	−25 ± 1	9 ± 2	80 ± 5	30 ± 3	17 ± 1	0.68 ± 0.04	103 ± 4	194 ± 11
	80–100	87 ± 15	20 ± 3	−24 ± 0	14 ± 3	94 ± 3	34 ± 5	20 ± 6	1.04 ± 0.06	104 ± 2	238 ± 6
700	0–20	80 ± 14	30 ± 9	−22 ± 0	22 ± 6	88 ± 2	34 ± 6	17 ± 5	0.57 ± 0.02	104 ± 4	210 ± 13
	20–40	77 ± 22	23 ± 6	−29 ± 1	14 ± 3	76 ± 4	31 ± 5	12 ± 2	0.84 ± 0.02	107 ± 3	224 ± 10
	40–60	89 ± 14	50 ± 12	−31 ± 3	9 ± 1	96 ± 3	41 ± 7	7 ± 1	0.49 ± 0.06	106 ± 2	219 ± 9
	60–80	79 ± 17	56 ± 14	−31 ± 3	9 ± 1	104 ± 2	38 ± 6	6 ± 1	0.52 ± 0.06	113 ± 3	224 ± 6
	80–100	84 ± 12	27 ± 6	−36 ± 5	13 ± 3	73 ± 4	46 ± 5	11 ± 3	0.56 ± 0.05	106 ± 3	217 ± 9
1 000	0–20	72 ± 13	25 ± 5	−31 ± 4	26 ± 5	79 ± 4	32 ± 7	23 ± 5	0.80 ± 0.11	105 ± 3	184 ± 8
	20–40	81 ± 11	43 ± 13	−31 ± 5	14 ± 2	58 ± 2	27 ± 6	9 ± 2	0.60 ± 0.07	106 ± 3	196 ± 12
	40–60	75 ± 10	59 ± 14	−30 ± 4	10 ± 2	88 ± 2	45 ± 5	7 ± 1	0.52 ± 0.05	103 ± 4	194 ± 8
	60–80	84 ± 7	62 ± 16	−30 ± 3	9 ± 1	101 ± 3	45 ± 4	10 ± 2	0.49 ± 0.02	100 ± 3	206 ± 13
	80–100	79 ± 12	53 ± 7	−30 ± 4	16 ± 4	92 ± 3	39 ± 3	9 ± 2	0.47 ± 0.03	101 ± 2	195 ± 6

[a)] Values are mean ± standard deviation ($n = 3$).
[b)] TOC = total organic C; Fe_t = total Fe; Fe_d = total free iron oxides; Fe_o = poorly crystalline iron oxides; Mn_t = total Mn; Al_t = total Al; Si_t = total Si.

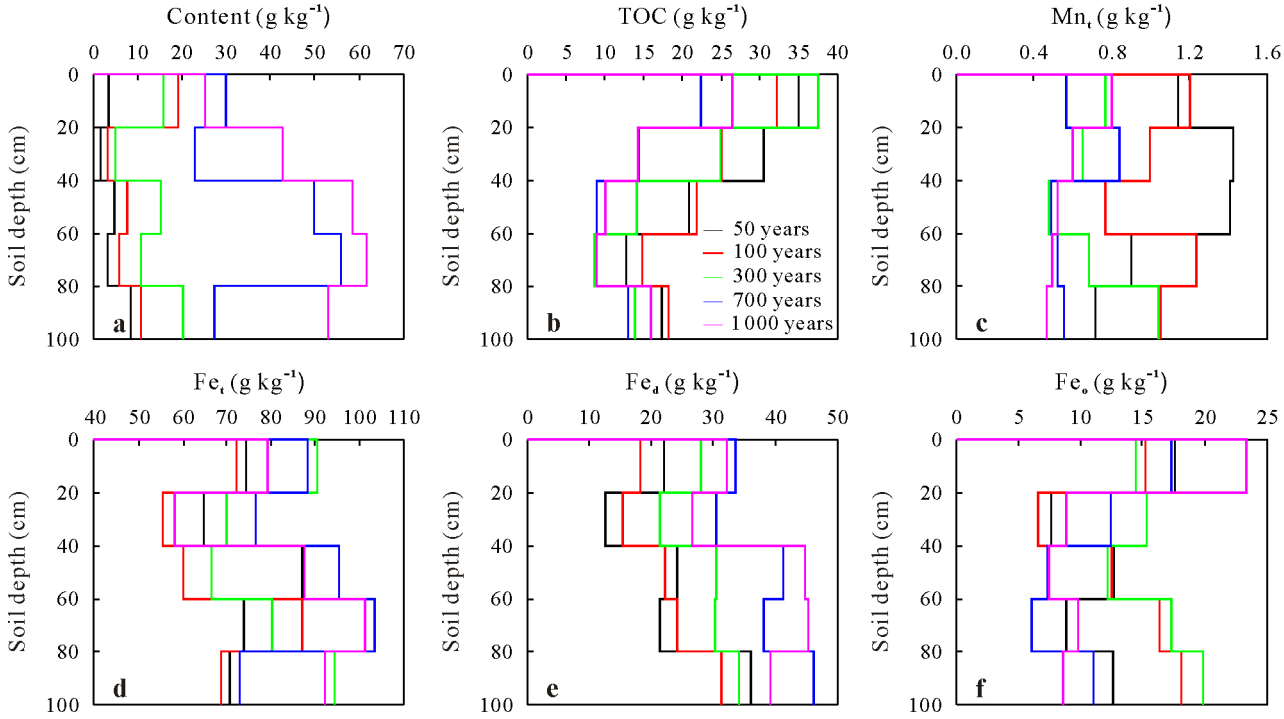

Fig. 1 Vertical distribution of natural nanoparticle (NNP) content (a) and contents of total organic C (TOC, b), total Mn (Mn_t, c), total Fe (Fe_t, d), total free iron oxides (Fe_d, e), and poorly crystalline iron oxides (Fe_o, f) of NNPs in the 1-m soil profiles under rice cultivation across a 1 000-year chronosequence in the coastal area of Cixi on the southern bank of Hangzhou Bay, Zhejiang Province, eastern China.

at a rate of approximately 60 g m^{-2} $year^{-1}$, of NNP stock in the 100-cm soil profile was found along the chronosequence ($R^2 = 0.93$, $P < 0.01$) (Fig. 2). The Fe_d and TOC stocks within the NNP fraction increased linearly at rates of 0.21 and 8 g m^{-2} $year^{-1}$, respectively. The stocks of Fe_t, Fe_o, and Mn_t within the NNPs also continuously accumulated with increasing cultivation age. The TEM images showed various NNP shapes consisting of irregular transparent and dark sheets (Fig. S3, see Supplementary Material for Fig. S3). The NNP size ranged from approximately 10 to 100 nm, and the larger sizes were attributed to agglomeration of NNPs upon drying for TEM analysis. In comparison, the mean hydrodynamic size of NNPs in the upper 0–20 cm topsoil varied from approximately 72 to 89 nm and decreased with increasing cultivation age (Table I).

Correlations among the bulk soil and NNP properties

Pearson correlations among the bulk soil and NNP properties were shown in Fig. 3 and Tables SIII and SIV (see Supplementary Material for Tables SIII and SIV). Soil cultivation age served as a keystone node in the correlation network, with a number of linkages to the bulk soil and NNP properties (Fig. 3). There were strong negative correlations between soil cultivation age and many bulk soil characteristics, including the silt content, EC, pH, and K^+, Na^+, and Ca^{2+}, and Mn_t contents. Notably, soil clay content was positively correlated with the cultivation age. Soil cultivation age was significantly correlated with soil NNP content and the contents of Fe_d and Fe_{do} in the NNPs ($r = 0.878$, 0.704, and 0.686, respectively), and they were positively correlated to each other ($r \geqslant 0.771$). Soil cultivation age exhibited a significant negative relationship with the size, zeta potential, and Mn_t content of the NNPs ($r = -0.733$, -0.750, and -0.701, respectively). Similarly, soil depth was significantly correlated with several bulk soil properties, including TOC, K^+, Mg^{2+}, Fe_d, and Fe_{do} contents, and with the TOC content of the NNPs.

Soil NNP content and the Fe_d and Fe_{do} contents in the NNPs were negatively correlated with soil silt content and EC and NNP zeta potential, but positively correlated with soil clay, Fe_d, and Fe_{do} contents ($P < 0.01$). The TOC contents of the NNPs were significantly correlated with those of the bulk soil samples ($r = 0.65$, $P < 0.01$). The TOC contents of the NNPs ranged from 8.7 to 37.6 g kg^{-1} and were higher in the topsoil horizons (0–40 cm) than the subsoil horizons. Higher TOC contents were observed in the NNPs (Table I) than in the bulk soil samples (3–20 g kg^{-1}, Table SII), indicating colloidal organic matter accumulation in the NNP fraction (Table I, Fig. 2).

As shown in Fig. 2, the Fe_d and Fe_{do} contents of the NNPs continuously increased with soil cultivation age. The distribution of Fe_d content of the NNPs was significantly correlated to that of the bulk soil samples ($r = 0.69$, $P <$

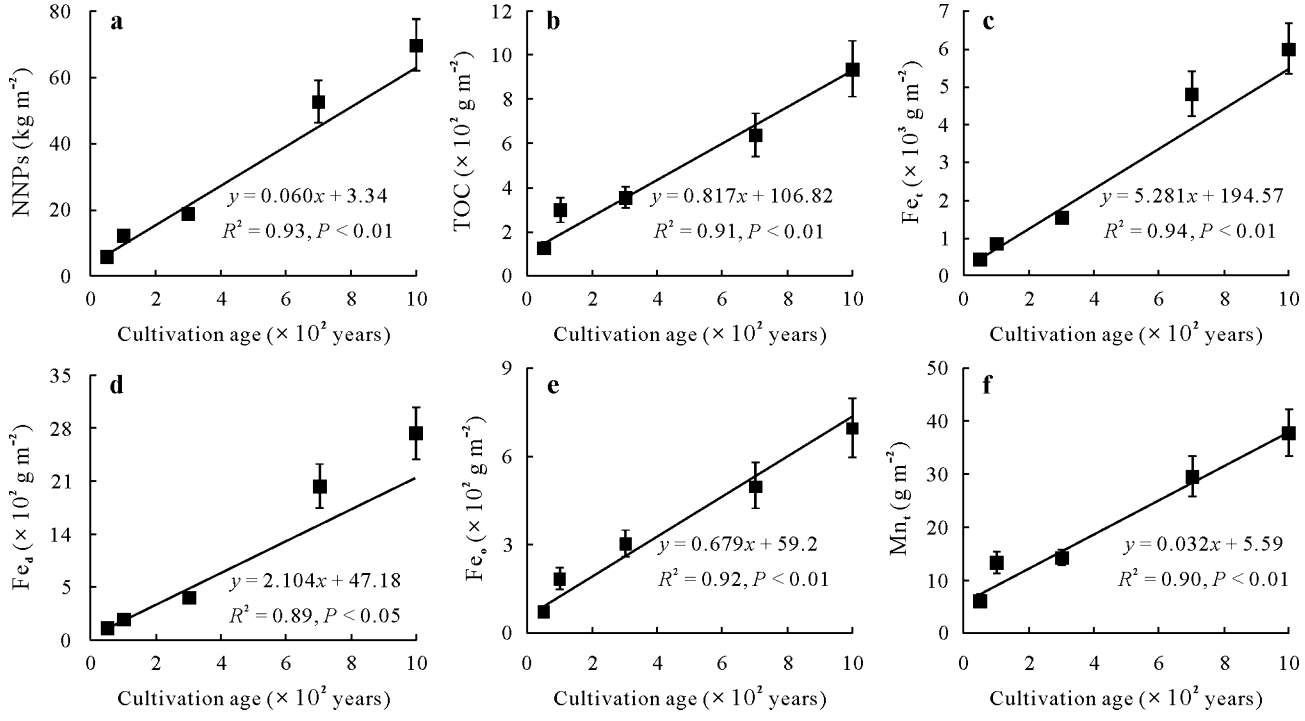

Fig. 2 Linear correlations between soil cultivation age and stocks of natural nanoparticles (NNPs) (a) and NPP total organic C (TOC, b), total Fe (Fe_t, c), total free iron oxides (Fe_d, d), poorly crystalline iron oxides (Fe_o, e), and total Mn (Mn_t, f) in the 1-m soil profiles under rice cultivation across a 1 000-year chronosequence in the coastal area of Cixi on the southern bank of Hangzhou Bay, Zhejiang Province, eastern China. Vertical bars are the standard deviations of means ($n = 3$).

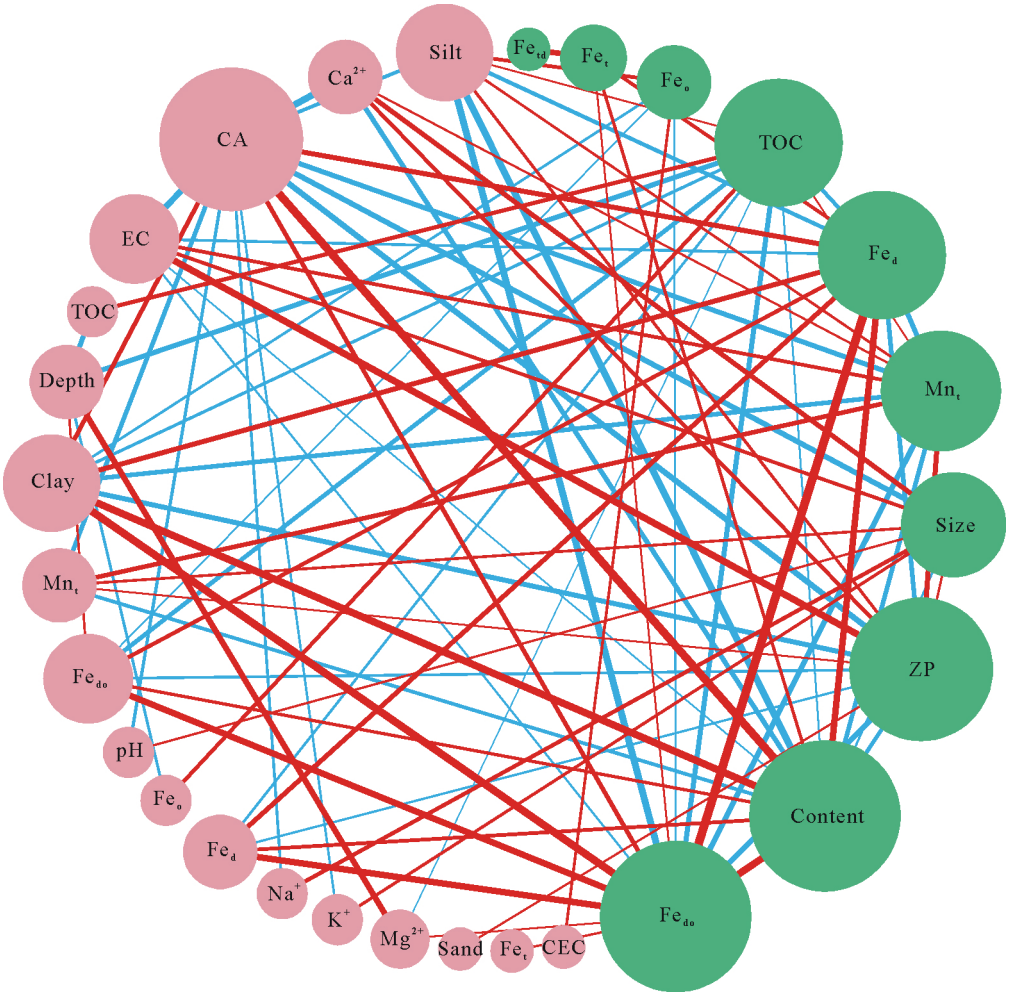

Fig. 3 Associations between bulk soil (pink) and soil natural nanoparticle (NNP) properties (green) visualized as a network based on Pearson correlation analysis. Only Pearson correlations at the Bonferroni-corrected level of $P < 0.01$ are depicted. Pearson correlation coefficient values are indicated by line width: the wider the line, the higher the correlation coefficient value (Tables SIII and SIV, See Supplementary Material for Tables SIII and SIV). Positive linkages are shown in red, and negative linkages are shown in blue. Node sizes are proportional to the number of correlations. CA = cultivation age; EC = electrical conductivity; TOC = total organic C; Mn_t = total Mn; Fe_{do} = crystalline oxides; Fe_o = poorly crystalline iron oxides; Fe_d = total free iron oxides; Fe_t = total Fe; ZP = zeta potential; CEC = cation exchange capacity; $Fe_{td} = Fe_t - Fe_d$.

0.01) (Table SIII). The Fe_o content of the NNPs was generally lower in the subsoil than in the topsoil horizons. However, in the younger soils (50–300 years), the Fe_o of the NNPs increased at the depth of 80–100 cm (Table I). The Fe_o content of the NNPs was correlated to the Fe_o content of the bulk soil samples ($r = 0.48$, $P < 0.05$). The Fe_{do} content of the NNPs also increased in deeper subsoil horizons after long-term paddy management and was correlated to that of the bulk soil samples ($r = 0.78$, $P < 0.01$). As shown in Fig. 1c, the Mn_t content of the NNPs decreased in the older soils (700–1 000 years) and was correlated to that of the bulk soil samples ($r = 0.67$, $P < 0.01$). Minimal changes were observed in the Al_t and Si_t contents of the NNPs.

To further determine the key bulk soil properties controlling changes in NNP properties, we employed RDA to quantify the role of bulk soil properties (Fig. 4). Significant factors were soil cultivation age, bulk density, and K^+ and Mg^{2+} contents. For the first two main axes, the RDA explained 68.9% and 7.4% of the variation in NNP properties, with the selected bulk soil properties accounting for 79.1% of this variance. The major portion of the variance was explained by soil cultivation age and extractable K^+ content on the first RDA axis, where 60.7% of the variation was explained by soil cultivation age. The second RDA axis was mainly related to soil bulk density and Mg^{2+} content.

Classification of soil cultivation age and soil depth groups based on NNP properties

Selected NNP properties were used to conduct the hierarchical cluster analysis. Based on the results, the samples were split into 50–300- and 700–1 000-year age groups in all soil layers (Fig. S4, see Supplementary Material for Fig. S4), which was different from the classification based on bulk soil properties. Details of the classification of age/depth groups

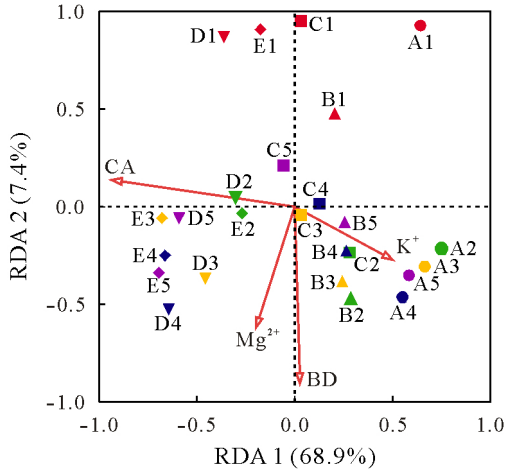

Fig. 4 Canonical redundancy analysis (RDA) plot of bulk soil and soil natural nanoparticle (NNP) properties. Letters A, B, C, D, and E next to the symbols indicate the soil cultivation ages of 50, 100, 300, 700, and 1 000, respectively. Numbers 1–5 associated with the letters A, B, C, D, and E correspond to sampling depths of 0–20, 20–40, 40–60, 60–80, and 80–100 cm, respectively. Different symbols and colors are used to distinguish samples of different soil cultivation ages and depths, respectively. Only bulk soil properties that significantly explained variability in NNP properties in the forward selection procedure were fitted to the ordination (red arrows). CA = cultivation age; BD = bulk density.

based on bulk soil properties are presented in SI. Specifically, the older soils (700–1 000 years) tended to show higher clay and NNP contents, accompanied by lower EC, pH, and NNP zeta potential values. Higher TOC contents were always found in the upper 0–20 cm topsoil, while higher clay, Fe_d, and NNP Fe_d contents were found at deeper subsoil in the older soils.

The PCA analysis was applied to further discriminate soil cultivation age and soil depth groups of the properties of NNPs in soil. The score plot (Fig. S5, see Supplementary Material for Fig. S5) revealed that the first two principal components (PCs) represented 78.2% and 10.5% of the total variance. The cumulative contribution of the first two PCs was 88.7%, which extensively described the soil cultivation age and soil depth groups of the NNPs. Soil NNPs were clearly split into 50–300-year and 700–1 000-year age groups (Fig. S5, see Supplementary Material for Fig. S5).

DISCUSSION

Distribution of NNPs across the soil chronosequence

Across the 1 000-year chronosequence, a longer soil cultivation resulted in increased NNP contents (Fig. 1a) and stocks (Fig. 2), especially in the subsoil horizons. Soil NNP contents shared a similar distribution trend with soil clay contents ($r = 0.83$, $P < 0.01$), which is consistent with previously reported correlations between the contents of water-dispersible colloids in NNPs and soil clay (Vendelboe *et al*., 2012). Both NNP and clay contents were strongly correlated with soil cultivation age ($r = 0.88$ and 0.68, respectively). Translocation of fine particles through dispersion and illuviation could influence the vertical distribution of NNPs in soils with increasing cultivation age. Downward translocation of particles in paddy soils may be attributed to pedogenic processes induced by long-term human activities, such as plowing, drainage, and flooding (Zhang and Gong, 2003).

Additional pedogenic processes associated with the redistribution of NNPs at the soil profile scale may result from human-induced changes in soil EC and NNP zeta potential. In the 1 000-year chronosequence, soil EC in the range of 172 to 1 297 μS cm^{-1} decreased with increasing soil cultivation age (Table SII) and showed a negative correlation with cultivation age ($r = -0.77$, $P < 0.01$) and NNP content ($r = -0.53$, $P < 0.01$). Similarly, the NNP zeta potential values were strongly correlated with soil EC ($r = 0.80$, $P < 0.01$). Jiang Y J *et al*. (2017) demonstrated with soil column experiments that NNP dispersion and transport were strongly enhanced in lower-ionic strength solutions. The NNP zeta potential values in the ranges from −22 to −36 mV also decreased with increasing soil cultivation age (Table I). Concomitant with the decrease in soil EC, soil K^+, Na^+, and Ca^{2+} contents decreased with time since the start of cultivation ($r = -0.54$, -0.56, and -0.80, respectively). These results suggest that the formation and redistribution of NNPs were strongly influenced by desalination and decalcification.

Previous studies on soil colloids indicated that low ionic strength could favor colloid mobilization in water-saturated columns (Zhang and Selim, 2007; Zhou *et al*., 2011). The sensitivity of colloidal dispersion to monovalent (*e.g*., Na^+, which enhances dispersion) *versus* divalent cations (*e.g*, Ca^{2+}, which promotes flocculation) also contributes to flocculation/dispersion dynamics (Shainberg *et al*., 1981). High electrolyte concentrations (*i.e*., high EC) decrease the thickness of the diffuse double layer of NNPs, leading to coagulation caused by enhanced van der Waals attraction (Li *et al*., 2016). When electrolyte concentrations increase, the absolute values of zeta potential become less than 30 mV (which is considered a threshold for NNP aggregate stability), resulting in a decrease in electrostatic repulsion (Zhu *et al*., 2014). As a result, illite and montmorillonite are susceptible to high electrolyte and Ca^{2+} in the younger soils promoting aggregation (Tombácz and Szekeres, 2004). Similarly, ionic strength could influence the heterocoagulation of iron oxides and other mineral particles (Sotirelis and Chrysikopoulos, 2017), which was also reflected in the relationship between iron oxides and NNPs in our study.

Before cultivation-induced desalinization/decalcification, high electrolyte concentrations maintained absolute values for NNP zeta potential of less than 30 mV resulting in the formation of stable NNP aggregates, which limited

the content of NNPs in the 1 000-year soil chronosequence. Accordingly, the wetland soil (0-year cultivation) had negligible extractable NNPs after ultrasonic treatment, in part due to the effects of high EC and Ca^{2+} content on formation of stable NNP aggregates. As soil cultivation age increased and desalinization/decalcification progressed, the decreases in ionic strength and Ca^{2+} content resulted in increased repulsive forces between mineral surfaces, promoting dispersion of NNP aggregates, which also contributed to decreased NNP size with increasing cultivation age (Miao *et al*., 2015). In addition, natural organic matter can enhance the water stability of NNPs, in which electrostatic repulsion plays an important role in interactions of NNPs (Zhu *et al*., 2017). This may partially explain the increase in NNP content as the TOC content of the NNPs increased during development in the soil chronosequence (Fig. 1b).

Results from Wissing *et al*. (2013) demonstrated that iron oxides strongly interacted with TOC and promoted accumulation of TOC in soil during rice cultivation. Since the Fe_o content of the NNPs was correlated to the TOC content of the NNPs ($r = 0.339$, Table SIV), the higher Fe_o proportion in the NNPs induced by long-term paddy soil cultivation (Fig. 2e) could similarly accelerate the accumulation of TOC in the NNPs. Additionally, TOC accumulation could impart highly negative zeta potentials to NNPs, increasing electrostatic repulsive forces between NNPs and thereby reducing their aggregation, as well as forming smaller and more stable NNPs (Miao *et al*., 2015; Li *et al*., 2016; Wang *et al*., 2019) with prolonged rice cultivation. As a result, NNP aggregates were dispersed as individual NNPs, contributing to the translocation and accumulation of NNPs predominantly in the subsoil horizons of the older (700–1 000 years) soils (Fig. 1a). Therefore, the changes in NNP content and profile distribution were appreciably influenced by human-induced changes in soil EC and NNP zeta potential during development of the soil chronosequence.

Changes of NNP properties across the soil chronosequence

Despite many years of rice cultivation, soil NNP, Al_t, and Si_t contents did not significantly change across the 1 000-year chronosequence (Table I). This is consistent with our previous research, which showed that the composition of soil NNPs was directly related to the properties of the parent material from which the soils were derived (Li *et al*., 2012). Chen *et al*. (2011) reported that 1 000 years of rice cultivation caused only small changes in aluminosilicate clay minerals. We found no clear trend for changes in the elemental composition of either the bulk soil or the NNPs across the soil chronosequence (Tables SII and I).

In contrast to elemental composition, some other NNP properties changed significantly during the 1 000 years of rice cultivation. The RDA analysis results demonstrated that soil cultivation age alone could explain up to 60.7% of the temporal variation in NNP properties (Fig. 4). The TOC, Fe_d, Fe_o, Fe_{do}, and Mn_t contents in the NNPs were positively correlated with those of the bulk soil (Fig. 3, Table SIII). Among these properties, changes in the Fe_t, Fe_d, Fe_o, and Fe_{do} contents were particularly evident and illustrated active chemical weathering and pedogenesis (Fig. 1). Both Fe_d and Fe_o accumulated in the NNPs of the older paddy soils (700–1 000 years) and increased with increasing cultivation age (Table I, Fig. 2). Furthermore, the Fe_{do} content of the NNPs was positively related with their Fe_d content ($r = 0.91$) and comprised the majority of NNP Fe_d in the subsoil horizons of the older paddy soils (700–1 000 years). Our results demonstrated that the Fe_{do} content of the NNPs had a stronger relationship with soil cultivation age ($r = 0.69$) than that of the bulk soil ($r = 0.37$) (Table SIII). The Fe_{do} fraction might interact with the microbial community by restraining the availability of substrate owing to organic matter sorption onto iron minerals (Dippold *et al*., 2014; Turner *et al*., 2019). Thus, the Fe_{do} of the NNPs may play an important role due to its large increase with soil cultivation age and its greater mobility (Liu *et al*., 2018). Redox cycles in paddy soils could lead to a higher proportion of Fe_o (poorly crystalline forms) (Wissing *et al*., 2014). Wissing *et al*. (2013) reported a higher proportion of Fe_o present in soil after approximately 50 years of paddy management. The distribution of Fe_t, Fe_d, Fe_o, and Fe_{do} of the NNPs suggested that redox processes were similarly affecting all of them. In addition, the Mn content of the NNPs decreased with increasing soil cultivation age ($r = -0.70$) (Table SIII). The more dynamic redox nature of Mn makes it more mobile than Fe under reducing conditions explaining the preferential loss of Mn from paddy soils (Huang *et al*., 2017). Eluviation of Mn began at the early stages of paddy management and commenced much earlier than the increase of Fe_d in the subsoil horizons.

Total organic C, as an organic matter property, accumulated in the NNPs of the upper 0–20 cm topsoil (Fig. 1b), and its content was negatively correlated with soil depth ($r = -0.70$). Pearson correlation analysis indicated that the NNP organic matter property was similar to that of the bulk soil across the 1 000-year chronosequence. Paddy management has been shown to slow decomposition and favor accumulation of soil organic matter (Sahrawat, 2004), and its accumulation in the topsoil horizons has been demonstrated for the entire period of paddy development (Kölbl *et al*., 2014; Wissing *et al*., 2014). After 50 years of cultivation, the differences in TOC between the topsoil and subsoil horizons became more evident (Chen *et al*., 2011). There was evidence for a more rapid increase of NNP TOC in the upper 0–20 cm topsoil within 50–300 years relative to that over 700–1 000 years (Fig. 1). In contrast, NNP TOC contents in the subsoil horizons changed only slightly throughout the soil chronosequence.

Implications of natural nanoparticle evolution in the 1 000-year soil chronosequence

The effects of long-term paddy management on reclaimed coastal soils were evident for bulk soil and NNP properties across the 1 000–year soil chronosequence. Categorization of pedogenic processes using cluster and PCA analyses (Figs. S4 and S5) divided the cumulative pedogenic processes into two periods. Cluster analysis for NNPs divided all soil layers of the chronosequence into periods of 50–300 years (T1) and 700–1 000 years (T2). In contrast, based on bulk soil, the period T1 included the 50–100-year topsoil horizon samples and the 50–700-year subsoil horizon samples, while the period T2 included the 100–1 000-year topsoil horizon samples and the 700–1 000-year subsoil horizon samples (Fig. S6). The difference between the two categorizations was due to delayed changes in NNP properties relative to those in the bulk soil properties.

Desalinization and decalcification are common phenomena that take place in land reclamation of coastal regions (Wissing *et al*., 2014). The high soil EC and Ca^{2+} content during the initial reclamation period led to a low NNP content, likely due to the formation of water-stable NNP aggregates. After the initial process of desalinization/decalcification within approximately 50 years, eluviation of Mn and accumulation of TOC were observed in the NNPs in the upper 0–20 cm topsoil. As soil EC and pH values continuously decreased during this period, NNP accumulation was initiated, which extended through the first stage (the period T1) of pedogenesis (50–300 years). At the second stage (the period T2), soil EC and pH values reached a steady state, which allowed for the dispersion of NNP aggregates leading to a relatively continuous increase in NNP content (60 g m^{-2} $year^{-1}$) over the 1 000-year chronosequence. In addition, the Fe_o and TOC contents preferentially increased in the upper 0–20 cm topsoil during this period. The accumulation of TOC in the NNPs owing to its association with Fe_o in the NNPs could be terminated by iron oxide leaching (Wissing *et al*., 2013). However, it did not occur even after 1 000 years of paddy management. These indicated that novel paddy management procedures (*e.g*., alternating wetting and drying) should be addressed in subsequent research, because paddy management alters redox conditions, as well as the iron oxide composition and its potential for organic C storage. Iron oxide accumulation and increased crystallization were evident in the subsoil horizons for both the NNPs and bulk soil. The changes in NNP properties were related to changes in the bulk soil properties. The changes in NNP properties were delayed relative to the changes in bulk soil properties, and thus the cluster analysis based on NNP properties divided pedogenesis into two distinct periods (50–300 and 700–1 000 years) in all soil layers. Given the significant impacts of paddy soils on global biogeochemical cycles and food production, appropriate water management to realize optimal EC, pH, and redox conditions in paddy soils during their millennial-scale evolution needs more attention.

CONCLUSIONS

Our investigation represents a first attempt to track NNP evolution during pedogenesis along a long-term (1 000 years) paddy soil chronosequence. We demonstrated that the distribution and properties of NNPs were strongly affected by long-term paddy soil cultivation in a chronosequence spanning 1 000 years. Some NNP properties, such as Fe and TOC contents, and profile distribution of NNPs changed considerably with increasing soil cultivation age and were in agreement with bulk soil properties as hypothesized. Long-term paddy management-initiated desalinization/decalcification, chemical weathering (especially Mn/Fe redox transformations), and pedogenesis may subsequently impact microbial communities and contaminant transport. Network and redundancy analyses indicated that soil cultivation age was the predominant factor affecting NNP properties, contributing to 60.7% of the total variability. In contrast, soil depth was not a dominant factor controlling variations in NNP properties. Overall, this study provides valuable insights into understanding how NNPs change over long-time periods and may be used to predict how NNP evolution over time might impact agricultural productivity and pollutant fate/transport. Future studies should cover a broader spectrum of soil types, looking for idiosyncrasies and commonalities, in an effort to create a holistic view of NNP evolution in soil environments.

ACKNOWLEDGEMENTS

This work is supported by the National Natural Science Foundation of China (Nos. 41721001 and 41130532). We would like to thank Mr. Kankan Zhao of Zhejiang University, China for assistance with network analysis.

SUPPLEMENTARY MATERIAL

Supplementary material for this article is available in the online version.

REFERENCES

Bakshi S, He Z L, Harris W G. 2014. A new method for separation, characterization, and quantification of natural nanoparticles from soils. *J Nanopart Res*. **16**: 2261.

Bakshi S, He Z L, Harris W G. 2015. Natural nanoparticles: Implications for environment and human health. *Crit Rev Environ Sci Tec*. **45**: 861–904.

Bastian M, Heymann S, Jacomy M. 2009. Gephi: An open source software for exploring and manipulating networks. *In* Association for the Advancement of Artificial Intelligence (AAAI) (ed.) Proceedings of the Third International AAAI Conference on Weblogs and Social Media. AAAI, San Jose. pp. 361–362.

Chen L M, Zhang G L, Effland W R. 2011. Soil characteristic response times and pedogenic thresholds during the 1000-year evolution of a paddy soil chronosequence. *Soil Sci Soc Am J*. **75**: 1807–1820.

Dippold M, Biryukov M, Kuzyakov Y. 2014. Sorption affects amino acid pathways in soil: Implications from position-specific labeling of alanine. *Soil Biol Biochem*. **72**: 180–192.

Guo Y K, Wu X G, Pan C H, Zhang J S. 2012. Numerical simulation of the tidal flow and suspended sediment transport in the Qiantang estuary. *J Waterw Port Coast Ocean Eng*. **138**: 192–202.

Han G Z, Zhang G L, Li D C, Yang J L. 2015. Pedogenetic evolution of clay minerals and agricultural implications in three paddy soil chronosequences of South China derived from different parent materials. *J Soil Sediment*. **15**: 423–435.

Hochella M F Jr, Lower S K, Maurice P A, Penn R L, Sahai N, Sparks D L, Twining B S. 2008. Nanominerals, mineral nanoparticles, and earth systems. *Science*. **319**: 1631–1635.

Hochella M F Jr, Spencer M G, Jones K L. 2015. Nanotechnology: Nature's gift or scientists' brainchild? *Environ Sci Nano*. **2**: 114–119.

Hochella M F Jr, Mogk D W, Ranville J, Allen I C, Luther G W, Marr L C, McGrail B P, Murayama M, Qafoku N P, Rosso K M, Sahai N, Schroeder P A, Vikesland P, Westerhoff P, Yang Y. 2019. Natural, incidental, and engineered nanomaterials and their impacts on the Earth system. *Science*. **363**: eaau8299.

Huang L M, Thompson A, Zhang G L, Chen L M, Han G Z, Gong Z T. 2015. The use of chronosequences in studies of paddy soil evolution: A review. *Geoderma*. **237-238**: 199–210.

Huang Q Y, Tang S H, Huang X, Zhang F B, Yi Q, Li P, Fu H T. 2017. Influence of rice cultivation on the abundance and fractionation of Fe, Mn, Zn, Cu, and Al in acid sulfate paddy soils in the Pearl River Delta. *Chem Geol*. **448**: 93–99.

Jiang J, Dai Z X, Sun R, Zhao Z J, Dong Y, Hong Z N, Xu R K. 2017. Evaluation of ferrolysis in arsenate adsorption on the paddy soil derived from an Oxisol. *Chemosphere*. **179**: 232–241.

Jiang Y J, Yu L, Sun H M, Yin X Q, Wang C Z, Mathews S, Wang N. 2017. Transport of natural soil nanoparticles in saturated porous media: Effects of pH and ionic strength. *Chem Spec Bioavail*. **29**: 186–196.

Kölbl A, Schad P, Jahn R, Amelung W, Bannert A, Cao Z H, Fiedler S, Kalbitz K, Lehndorff E, Müller-Niggemann C, Schloter M, Schwark L, Vogelsang V, Wissing L, Kögel-Knabner I. 2014. Accelerated soil formation due to paddy management on marshlands (Zhejiang Province, China). *Geoderma*. **228-229**: 67–89.

Leff B, Ramankutty N, Foley J A. 2004. Geographic distribution of major crops across the world. *Global Biogeochem Cycles*. **18**: GB1009.

Li S B, Ma H B, Wallis L K, Etterson M A, Riley B, Hoff D J, Diamond S A. 2016. Impact of natural organic matter on particle behavior and phototoxicity of titanium dioxide nanoparticles. *Sci Total Environ*. **542**: 324–333.

Li W, He Y, Wu J, Xu J. 2012. Extraction and characterization of natural soil nanoparticles from Chinese soils. *Eur J Soil Sci*. **63**: 754–761.

Liu F, Xu B L, He Y, Brookes P C, Tang C X, Xu J M. 2018. Differences in transport behavior of natural soil colloids of contrasting sizes from nanometer to micron and the environmental implications. *Sci Total Environ*. **634**: 802–810.

Liu F, Xu B L, He Y, Brookes P C, Xu J M. 2019. Co-transport of phenanthrene and pentachlorophenol by natural soil nanoparticles through saturated sand columns. *Environ Pollut*. **249**: 406–413.

Liu G, Ma J, Yang Y T, Yu H Y, Zhang G B, Xu H. 2019. Effects of straw incorporation methods on nitrous oxide and methane emissions from a wheat-rice rotation system. *Pedosphere*. **29**: 204–215.

Liu Y, Dong Y, Wang P, Hussain Q, Ge T, Wang J. 2019. Distribution of methane production and methanogenic archaeal community structure across soil particle size fractions along a rice chronosequence. *J Soil Water Conserv*. **74**: 235–246.

Miao L Z, Wang C, Hou J, Wang P F, Ao Y H, Dai S S, Lv B W. 2015. Effects of pH and natural organic matter (NOM) on the adsorptive removal of CuO nanoparticles by periphyton. *Environ Sci Pollut Res*. **22**: 7696–7704.

Qian H Y, Huang S, Chen J, Wang L, Hungate B A, Van Kessel C, Zhang J, Deng A X, Jiang Y, Van Groenigen K J, Zhang W J. 2020. Lower-than-expected CH_4 emissions from rice paddies with rising CO_2 concentrations. *Glob Chang Biol*. **26**: 2368–2376.

Rod K, Um W, Chun J, Wu N, Yin X L, Wang G H, Neeves K. 2018. Effect of chemical and physical heterogeneities on colloid-facilitated cesium transport. *J Contam Hydrol*. **213**: 22–27.

Shainberg I, Rhoades J D, Prather R J. 1981. Effect of low electrolyte concentration on clay dispersion and hydraulic conductivity of a sodic soil. *Soil Sci Soc Am J*. **45**: 273–277.

Soil Survey Staff. 2014. Keys to Soil Taxonomy. 12th Edn. USDA-Natural Resources Conservation Service, Washington, D.C.

Song Y, Bian Y R, Wang F, Herzberger A, Yang X L, Gu C G, Jiang X. 2017. Effects of biochar on dechlorination of hexachlorobenzene and the bacterial community in paddy soil. *Chemosphere*. **186**: 116–123.

Sotirelis N P, Chrysikopoulos C V. 2017. Heteroaggregation of graphene oxide nanoparticles and kaolinite colloids. *Sci Total Environ*. **579**: 736–744.

Sahrawat K L. 2004. Organic matter accumulation in submerged soils. *Adv Agron*. **81**: 169–201.

Taghipour M, Jalali M. 2018. Heavy metal release from some industrial wastes: Influence of organic and inorganic acids, clay minerals, and nanoparticles. *Pedosphere*. **28**: 70–83.

Theng B K G, Yuan G D. 2008. Nanoparticles in the soil environment. *Elements*. **4**: 395–399.

Tombácz E, Szekeres M. 2004. Colloidal behavior of aqueous montmorillonite suspensions: The specific role of pH in the presence of indifferent electrolytes. *Appl Clay Sci*. **27**: 75–94.

Turner S, Mikutta R, Guggenberger G, Schaarschmidt F, Schippers A. 2019. Distinct pattern of nitrogen functional gene abundances in top- and subsoils along a 120, 000-year ecosystem development gradient. *Soil Biol Biochem*. **132**: 111–119.

Van Den Bogaert R, Labille J, Cornu S. 2015. Aggregation and dispersion behavior in the 0- to 2-μm fraction of Luvisols. *Soil Sci Soc Am J*. **79**: 43–54.

Vendelboe A L, Moldrup P, Schjønning P, Oyedele D J, Jin Y, Scow K M, De Jonge L W. 2012. Colloid release from soil aggregates: Application of laser diffraction. *Vadose Zone J*. **11**: 120–128.

Wang X N, Wang S, Pan X L, Gadd G M. 2019. Heteroaggregation of soil particulate organic matter and biogenic selenium nanoparticles for remediation of elemental mercury contamination. *Chemosphere*. **221**: 486–492.

Watanabe T, Asakawa S, Hayano K. 2020. Long-term submergence of non-methanogenic oxic upland field soils helps to develop the methanogenic archaeal community as revealed by pot and field experiments. *Pedosphere*. **30**: 62–72.

Wei C L, Gao W D, Whalley W R, Li B G. 2018. Shrinkage characteristics of lime concretion black soil as affected by biochar amendment. *Pedosphere*. **28**: 713–725.

Wissing L, Kölbl A, Häusler W, Schad P, Cao Z H, Kögel-Knabner I. 2013. Management-induced organic carbon accumulation in paddy soils: The role of organo-mineral associations. *Soil Tillage Res*. **126**: 60–71.

Wissing L, Kölbl A, Schad P, Bräuer T, Cao Z H, Kögel-Knabner I. 2014. Organic carbon accumulation on soil mineral surfaces in paddy soils derived from tidal wetlands. *Geoderma*. **228-229**: 90–103.

Xie D F, Wang Z B, Gao S, De Vriend H J. 2009. Modeling the tidal channel morphodynamics in a macro-tidal embayment, Hangzhou Bay, China. *Cont Shelf Res*. **29**: 1757–1767.

Xie D F, Pan C H, Wu X G, Gao S, Wang Z B. 2017. Local human activities overwhelm decreased sediment supply from the Changjiang River: Continued rapid accumulation in the Hangzhou Bay-Qiantang Estuary system. *Mar Geol*. **392**: 66–77.

Xu B L, Lian Z H, Liu F, Yu Y J, He Y, Brookes P C, Xu J. 2019. Sorption of pentachlorophenol and phenanthrene by humic acid-coated hematite nanoparticles. *Environ Pollut*. **248**: 929–937.

Zhang G L, Gong Z T. 2003. Pedogenic evolution of paddy soils in different soil landscapes. *Geoderma*. **115**: 15–29.

Zhang H, Selim H M. 2007. Colloid mobilization and arsenite transport in soil columns: Effect of ionic strength. *J Environ Qual*. **36**: 1273–1280.

Zhang W, Tang X Y, Xian Q S, Weisbrod N, Yang J E, Wang H L. 2016. A field study of colloid transport in surface and subsurface flows. *J Hydrol*. **542**: 101–114.

Zhou D M, Wang D J, Cang L, Hao X Z, Chu L Y. 2011. Transport and re-entrainment of soil colloids in saturated packed column: Effects of pH and ionic strength. *J Soil Sediment*. **11**: 491–503.

Zhou H, Fang H, Mooney S J, Peng X H. 2016. Effects of long-term inorganic and organic fertilizations on the soil micro and macro structures of rice paddies. *Geoderma*. **266**: 66–74.

Zhu X, Chen H, Li W, He Y, Brookes P C, Xu J. 2014. Aggregation kinetics of natural soil nanoparticles in different electrolytes. *Eur J Soil Sci*. **65**: 206–217.

Zhu X, Chen H, Li W, He Y, Brookes P C, White R, Xu J M. 2017. Evaluation of the stability of soil nanoparticles: The effect of natural organic matter in electrolyte solutions. *Eur J Soil Sci*. **68**: 105–114.

Zhu Z K, Ge T D, Liu S L, Hu Y J, Ye R Z, Xiao M L, Tong C L, Kuzyakov Y, Wu J S. 2018. Rice rhizodeposits affect organic matter priming in paddy soil: The role of N fertilization and plant growth for enzyme activities, CO_2 and CH_4 emissions. *Soil Biol Biochem*. **116**: 369–377.